I&EC research
Industrial & Engineering Chemistry Research

ARTICLE

pubs.acs.org/IECR

Effect of Nano-TiO_2 Particles on the Performance of PVDF, PVDF-*g*-(Maleic anhydride), and PVDF-*g*-Poly(acryl amide) Membranes

Xiaokai Bian,[†,‡] Liuqing Shi,[‡] Xuanxuan Yang,[†] and Xiaofeng Lu[‡,*]

[†]Graduate School of the Chinese Academy of Sciences, Beijing 100049, China

[‡]Shanghai Institute of Applied Physics, Chinese Academy of Sciences, Shanghai 201800, China

ABSTRACT: To study the effects of nano-TiO_2 particles on membrane performance and structure and to explore possible interactions between nano-TiO_2 particles and polymer, polymer/TiO_2 embedded hybrid membranes and neat polymer membranes were prepared using the phase inversion method. Poly(vinylidene difluoride) (PVDF), poly(vinylidene difluoride)-*g*-(maleic anhydride) (PVDF-*g*-MA), and poly(vinylidene difluoride)-*g*-poly(acryl amide) (PVDF-g-PAM) were selected as the membrane materials. SEM images showed that the hybrid membranes had a thinner skin layer and a larger number of pores in the sublayer than the neat membranes, which was the main cause of the increase in water flux of the hybrid membranes. They also exhibited a better antifouling property than the neat ones in the continuous BSA solution filtration process. In the 48-h-long pure-water experiment, the hybrid membranes underwent a water flux decline and an increase in contact angle. The loss of nano-TiO_2 particles, revealed by EDS analysis, influenced the stability of hybrid membrane performance. The XPS analysis suggested that nano-TiO_2 particles were immobilized in the membrane surface layer through the formation of a stable chemical structure resulting from its reaction with polymer and/or through intertwining with polymer chains.

1. INTRODUCTION

In 1990, Doyen and colleagues prepared an organic−inorganic membrane by adding ZrO_2 inorganic particles to a polymer membrane.[1] The subsequent two decades have seen the publication of studies of hybrid membranes, one after another. Hybrid membranes have found wide application in processes such as reverse osmosis (RO), gas separation, pervaporation, nanofiltration, and ultrafiltration (UF).[2−15] Almost all common polymer membrane materials, such as polysulfone, poly(ether sulfone), poly(vinyl alcohol), poly(vinylidene difluoride), polyimide, and poly(acrylonitrile), have been used as polymer matrixes to form hybrid membranes, and the inorganic materials added to the polymer matrix have included ZrO_2, Al_2O_3, SiO_2, TiO_2, and Fe_3O_4.

With the rapid development of nanotechnology, the size of the added inorganic particles has moved from the micrometer to the nanometer scale. Owing to their ultrasmall size, nanoparticles take on many special characteristics. Among nanoparticles, TiO_2 exhibits superior photocatalysis and hydrophilicity and is drawing increasing attention for membrane surface modification purposes. Molinari et al. prepared organic−inorganic membranes such as TiO_2-deposited membranes and TiO_2-embedded membranes, whose photobactericidal and photocatalytic properties brought about by the nanoparticles immobilized in the membranes were exploited for water purification.[16−18] With the deepening understanding of the hydrophilicity of TiO_2, its nanoparticles have been used in the preparation of antifouling membranes. Bae and Tak prepared TiO_2-entrapped and TiO_2-deposited UF membranes.[19] Both membranes exhibited an antifouling nature. It was also found that the TiO_2-deposited membrane exhibited a better fouling mitigation performance, whereas the TiO_2-entrapped membrane demonstrated better stability.

Some membrane researchers have reported that the adhesion of nanoparticles is an important factor affecting the stability of hybrid membranes. To improve membrane stability and strengthen the interaction between the nanoparticles the and polymer, the concept of self-assembly was introduced into the preparation of membranes. For example, Shin et al.[20,21] fabricated TiO_2 thin films through self-assembly monolayer adsorption on $-SO_3$-functionalized surfaces; Liu and co-workers took advantage of the static adsorption between the positive TiO_2 complex in acidic solution and the negative poly(sodium 4-styrenesulfonate) (PSS) surface to construct molecular-level ordered TiO_2/PSS films by a layer-by-layer self-assembly process.[22] It has also been reported that self-assembly can occur between nano-TiO_2 particles and carboxylate (−COOH) groups or sulfonic acid ($-SO_3H$) groups. Kwak et al. obtained hybrid aromatic polyamide membranes through self-assembly of TiO_2 nanoparticles on polymer chains with −COOH groups along the membrane surface that exhibited improved antifouling properties. Most importantly, XPS data indicated in a quantitive manner that the nano-TiO_2 particles introduced into the membrane surface were tightly self-assembled even under very harsh RO operating conditions.[2,3] Bae and Tak prepared nanocomposite membranes by immobilizing nano-TiO_2 particles onto sulfonate PES UF membranes to investigate the fouling mitigation effect of TiO_2 in activated sludge filtration.[19,23] Their results also suggested that the self-assembled nanoparticles were firmly attached to the membrane surface.

Received: January 31, 2011
Accepted: September 9, 2011
Revised: August 28, 2011
Published: September 09, 2011

dx.doi.org/10.1021/ie200232u | *Ind. Eng. Chem. Res.* 2011, 50, 12113–12123

Table 1. Compositions and Viscosities of Casting Solutions for Neat and Hybrid Membranes

membrane ID	casting solution composition (wt %)			TiO_2[a] (g)	casting solution viscosity[b] (cP)
	polymer	PEG400	NMP		
PVDF	PVDF 24	5	71	0	4697
PVDF/TiO_2-0.04				0.04	5058
PVDF/TiO_2-0.1				0.1	5153
PVDF/TiO_2-0.14				0.14	5274
PVDF/TiO_2-0.2				0.2	5351
PVDF-*g*-MA	PVDF-*g*-MA 22	5	73	0	2396
PVDF-*g*-MA/TiO_2-0.1				0.1	2407
PVDF-*g*-MA/TiO_2-0.2				0.2	2761
PVDF-*g*-MA/TiO_2-0.3				0.3	3228
PVDF-*g*-MA/TiO_2-0.4				0.4	4198
PVDF-*g*-PAM	PVDF-*g*-PAM 20	5	75	0	3574
PVDF-*g*-PAM/TiO_2-0.08				0.08	4053
PVDF-*g*-PAM/TiO_2-0.16				0.16	5006
PVDF-*g*-PAM/TiO_2-0.32				0.32	5286
PVDF-*g*-PAM/TiO_2-0.4				0.4	5359

[a] Amount of TiO_2 referenced to the amount of TiO_2 (in grams) added to 40 g of neat casting solution containing polymer, PEG400, and NMP only. [b] Shear rate = 100 s^{-1}.

This study is an attempt to investigate the modification effect of nano-TiO_2 particles on membrane performance and structure and to discuss possible interactions between nano-TiO_2 particles and functional groups other than −COOH and $-SO_3H$ groups and their effects on the stability of hybrid membrane performance. To this end, nano-TiO_2 in different amounts was blended with PVDF and PVDF with functional groups (i.e., PVDF-*g*-MA and PVDF-*g*-PAM) to form embedded polymer/TiO_2 hybrid membranes. Neat membranes (i.e., membranes without TiO_2 addition) were also prepared. Membrane performance tests were carried out, and the morphologies of the membranes were investigated by scanning electron microscopy (SEM). Water contact angles of the membranes were measured to evaluate the hydrophicility of the membrane surfaces. X-ray photoelectron spectroscopy (XPS) was employed for the analysis of possible interactions between nano-TiO_2 and polymer and energy-dispersive X-ray spectroscopy (EDS) and energy-dispersive X-ray mapping (EDX mapping) were used to analyze the Ti content and Ti distribution in the membrane surface.

2. EXPERIMENTAL SECTION

2.1. Materials. Poly(vinylidene difluoride) (PVDF) (KYNAR, 761) and poly(vinylidene difluoride)-*g*-(maleic anhydride) (PVDF-*g*-MA) [KYNAR(R) ADX 161] were purchased from Arkema Inc., and the degree of grafting (DG) of maleic anhydride in the latter was 0.1%. Poly(vinylidene difluoride)-*g*-poly(acryl amide) (PVDF-*g*-PAM) powder was kindly supplied by Prof. Jingye Li of Shanghai Institute of Applied Physics; it was synthesized by irradiation-induced graft polymerization technique and had a DG of 0.4%.[24,25] *N*-Methyl-2-pyrrolidone (NMP) of analytical grade, poly(ethylene glycol) with a molecular weight (MW) of 400 g/mol (PEG400), and bovine serum albumin (BSA, MW = 67000 Da) were purchased from Sinopharm Chemical Reagent Co., Ltd. Nano-TiO_2 (particle size, 40−80 nm) was kindly provided by Shanghai Leizhen Chemical Products Company. PE nonwoven fabric (TYVEK 1057 D) was obtained from DuPont Co.

2.2. Membrane Preparation. Both hybrid membranes and membranes without nano-TiO_2 addition (referred to as neat membranes in this work) were prepared using the phase inversion method.

2.2.1. Preparation of Neat Membranes. The casting solution, which was prepared with a certain amount of polymer dissolved in NMP solvent with PEG400 as an additive at 70 °C, was applied to the surface of a nonwoven fabric of area 120 mm × 160 mm, with a scraper with a 0.2-mm gap at ambient temperature (24 °C) and humidity (53−54%), and then it was immediately immersed in a water coagulation bath at 20 °C to form neat membranes. The neat membranes thus obtained were then rinsed and stored in deionized water for later use. Detailed information on the components of the casting solution is provided in Table 1.

2.2.2. Preparation of Hybrid Membranes. Hybrid membranes were prepared in the same way as neat membranes, except that TiO_2 nanoparticles were added to the casting solution under vigorous stirring after the polymer had completely dissolved. Moreover, ultrasonic vibration was used to ensure that the particles were evenly dispersed in the casting solution, which was later kept in darkness for more than 24 h to eliminate the bubbles. The amount of TiO_2 addition is included in Table 1 as well.

2.2.3. Measurement of Casting Solution Viscosity. The viscosity of the casting solution was measured with a rotational rheometer (Advanced Rheology Expanded System, TA Instruments, Twin Lakes, WI) in the coaxial cylinder geometry. The temperature of the unit was controlled at 25 °C by a circulating water system. The casting solution was placed in the cylinder, and sufficient time was allowed for it to reach thermal equilibrium. The shear stress was determined up to shear rates of 100 s^{-1}.

2.3. Membrane Characterization. *2.3.1. SEM Morphology and EDX Mapping of Neat and Hybrid Membranes.* SEM (LEO Elektronenmikroskopie GmbH, Oberkochen, Germany) was

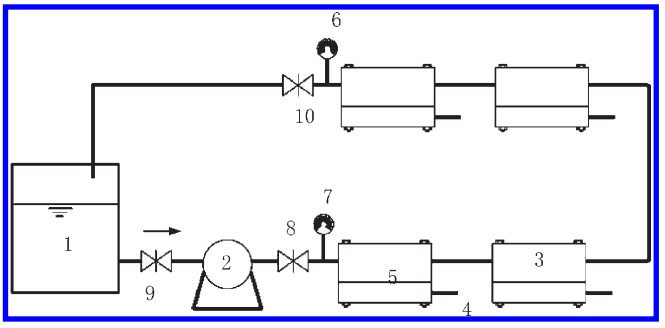

Figure 1. Schematic diagram of UF evaluation cells of four membranes in series: (1) feed tank, (2) pump, (3) membrane evaluation cell, (4) outlet for the permeate, (5) membrane, (6, 7) pressure gauges, (8) pressure control valve, (9, 10) valves.

used to observe the morphologies of membranes' surface and cross section. In the sample preparation, the membranes were immersed in liquid nitrogen, and the cross-sectional samples were obtained by fracturing. After being placed in a vacuum for drying, the samples were sputtered with Au and then placed into the chamber of SEM.

EDS was used to analyze the composition and Ti content of the membrane surface layer, and the analysis area was 100 × 70 μm. EDX mapping was used to evaluate the distribution of Ti in the surface of the hybrid membranes.

2.3.2. Pore Size Measurements. The average pore sizes of neat and hybrid membranes were measured with a self-made gas−liquid displacement instrument. A membrane sample cut into a circular shape was immersed in isopropanol for about 10 min until it reached a status of semitransparency; then, the sample was taken out, and the liquid on its surface was removed. After that, the sample was spread flat on the measurement instrument for analysis, with nitrogen used as a pressure source.

2.3.3. Filtration Tests. At room temperature, a self-made membrane evaluation cell was used to test the properties of both neat and hybrid membranes. The effective membrane area was 18.6 cm^2. (See Figure 1.) The peristaltic pump was adjusted to provide a test pressure of 0.2 MPa, and the measurement of the membrane surface cross-flow velocity was 1 m/s.

In this article, all values reported for flux are the averages of results obtained from four repeated tests.

2.3.3.1. Water Flux Measurements. Water flux was calculated according to the equation

$$\text{flux} = \frac{\text{permeate volume}}{\text{membrane effective area}} \times \text{time}\ (\text{L m}^{-2}\ \text{h}^{-1}) \quad (1)$$

where the permeate volume is the volume of permeate that penetrated the membrane during a certain period of time after the membrane had been precompacted under 0.2 MPa for 30 min.

2.3.3.2. Evaluation of Antifouling Properties of Neat and Hybrid Membranes. In this study, to compare the antifouling properties of neat and hybrid membranes, a filtration test that lasted continuously for 12 h under a pressure of 0.2 MPa was carried out, using a 0.5 g/L BSA solution (pH 7.4) as the feed solution. During this test, each membrane was precompacted by filtration of deionized water under a pressure of 0.2 MPa for 30 min, followed by filtration of deionized water under a pressure of 0.2 MPa for 5 h, and then its flux (F_{H_2O}) was recorded. Then, BSA solution was used as the feed, and the BSA flux (F_{BSA}) was

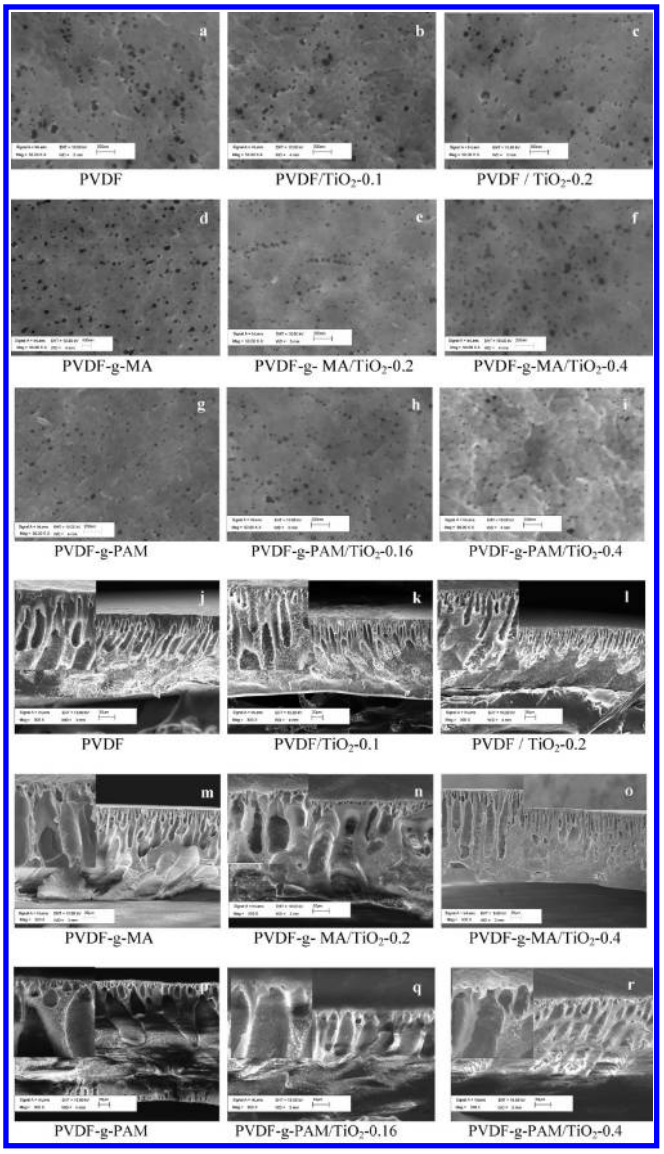

Figure 2. (a−i) Surface (50000×) and (j−r) cross-sectional (300×) SEM images of neat and hybrid membranes. The insets in the cross-sectional images show upper part of hybrid membrane structure at high magnification.

recorded at a regular interval of time. During this process, all of the penetrant flowed back to the feed bank to maintain the stability of the BSA concentration in the feed solution.

2.3.3.3. Evaluation of Performance Stability of Hybrid Membranes. In this study, to characterize the influence of nano-TiO_2 on the stability of hybrid membrane performance, its pure-water flux change over a 48-h operation period was monitored by taking measurements of the permeate volume at regular intervals during the operation so as to calculate its pure-water flux using eq 1. Meanwhile, at the end of certain operation periods, sample membranes were removed for the EDS analysis of the Ti content in the surface.

2.3.4. Contact Angle Measurements. The contact angles of the membranes were measured on an Attension Theta system (KSV Instruments Ltd., Helsinki, Finland). A water drop (4.0 μL) was lowered onto the sample membrane's surface from a needle tip. A magnified image of the droplet was recorded with a

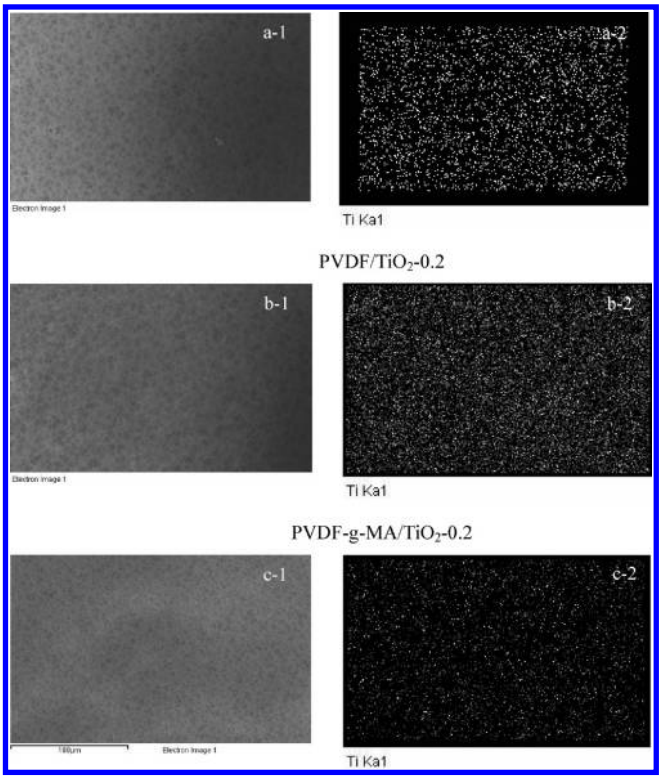

Figure 3. EDX mapping images of hybrid membranes (a) PVDF/TiO_2-0.2, (b) PVDF-*g*-MA/TiO_2-0.2, and (c) PVDF-*g*-PAM/TiO_2-0.16. The images on the left show the hybrid membrane surfaces.

digital camera. Static contact angles were determined from these images with calculation software. The contact angle measurements were taken as the mean values of seven different points on each membrane. In this article, the water contact angles of neat and hybrid membranes, as well as the contact angles of hybrid membranes after 48-h pure-water permeation experiments, were measured.

2.3.5. XPS Analysis. XPS experiments were carried out on an RBD upgraded PHI-5000C ESCA system (Perkin-Elmer) with Mg Kα radiation ($h\nu$ = 1253.6 eV) or Al Kα radiation ($h\nu$ = 1486.6 eV). The X-ray anode was run at 250 W, and the high voltage was kept at 14.0 kV with the detection angle at 54°. The pass energy was fixed at 23.5, 46.95, or 93.90 eV to ensure sufficient resolution and sensitivity. The base pressure of the analysis chamber was about 5×10^{-8} Pa. The sample was directly pressed into a self-supported disk (10 × 10 mm) and mounted on a sample holder, after which it was transferred into the analysis chamber. The overall spectrum [0−1100 (1200) eV] and the narrow spectra of all of the elements with much higher resolution were both recorded by using the RBD 147 interface (RBD Enterprises, Bend, OR) through the AugerScan 3.21 software. Binding energies were calibrated by using the containment carbon (C 1s = 284.6 eV). The data analysis was carried out using XPSPeak4.1 software provided by Raymund W. M. Kwok (The Chinese University of Hong Kong, Hong Kong, China).

3. RESULTS AND DISCUSSION

3.1. Morphologies and Structures of Neat and Hybrid Membranes. The effects of the addition of nano-TiO_2 particles on the membrane structure were observed by SEM. Figure 2 shows the surface and cross-sectional SEM images for both neat and hybrid membranes.

In terms of membrane surface structure, pores obviously exist on the membrane surface. However, no apparent difference in surface structure was found between neat and hybrid membranes. No obvious TiO_2 distribution was observed on the membrane surface; the particles might be wrapped up in the polymer. To understand the TiO_2 distribution inside the membrane, three groups of hybrid membranes were chosen for EDX mapping surface analysis. EDX mapping was performed on the surface of hybrid membranes. Figure 3 indicates that nano-TiO_2 particles were uniformly embedded in the near-surface area.

The cross-sectional images in Figure 2 indicate that both neat and hybrid membranes exhibited a typical asymmetric structure composed of a dense surface layer and a porous sublayer. In comparison with those in the neat membrane, the fingerlike pores in the sublayer of the hybrid membrane were small in size but existed in large quantities. The formation of large macrovoids was suppressed. The magnified images of the upper part of hybrid membrane structure show that, with an increase in the TiO_2 content, the skin layer decreased in thickness, the number of the pores increased, and the connectivity between the pores improved, particularly in the case of PVDF/TiO_2 hybrid membranes. Apparently, the addition of TiO_2 affected the membrane formation process. As the membrane skin layer was formed within a very short period of time, the casting solution containing nano-TiO_2, which has a high affinity for water and therefore accelerated the diffusion of solvent and nonsolvent during phase separation, prompted a rapid entry of polymer solution into the liquid−liquid demixing gap where phase separation takes place, polymer precipitates rapidly at the interface of solvent and nonsolvent, and hence the skin layer is thinner. Bae and Tak obtained similar results in the preparation of PSf−TiO_2 membranes.[19] The formation of the sublayer takes a longer time, and the form of its structure is influenced to a larger degree by the change in viscosity of the casting solution caused by the addition of nano-TiO_2. According to the theory on the formation of macrovoids proposed by McKelvey and Koros, macrovoids are initiated by nucleation of the polymer-lean phase, and their growth depends on the difference between the indiffusion rate of nonsolvent to dopant and the diffusion rate of the solvent to coagulation bath. This difference induced a nonsolvent concentration gradient in the casting solution, which is the driving force for the growth of macrovoids.[26] In this article, as seen from Table 1, the viscosities of the casting solutions increased with increasing TiO_2 content. This increase in viscosity of the casting solution decreased the diffusion rate of nonsolvent and the phase separation process tended toward a delayed demixing process, resulting in the suppression of macrovoids in the sublayer. Therefore, the size of macrovoids in the sublayer was smaller, but their number increased.

3.2. Effect of the Addition of Nano-TiO_2 Particles on Membrane Performance. *3.2.1. Filtration Performance.* To investigate the influence of nano-TiO_2 addition on membrane performance, hybrid membranes were prepared using casting solutions containing different amounts of nano-TiO_2 particles varying from 0.04 to 0.4 g. Within this concentration range, nano-TiO_2 particles could be well-dispersed in the casting solutions. Figure 4 shows the effects of different amounts of nano-TiO_2 particles on membrane performance. Table 2

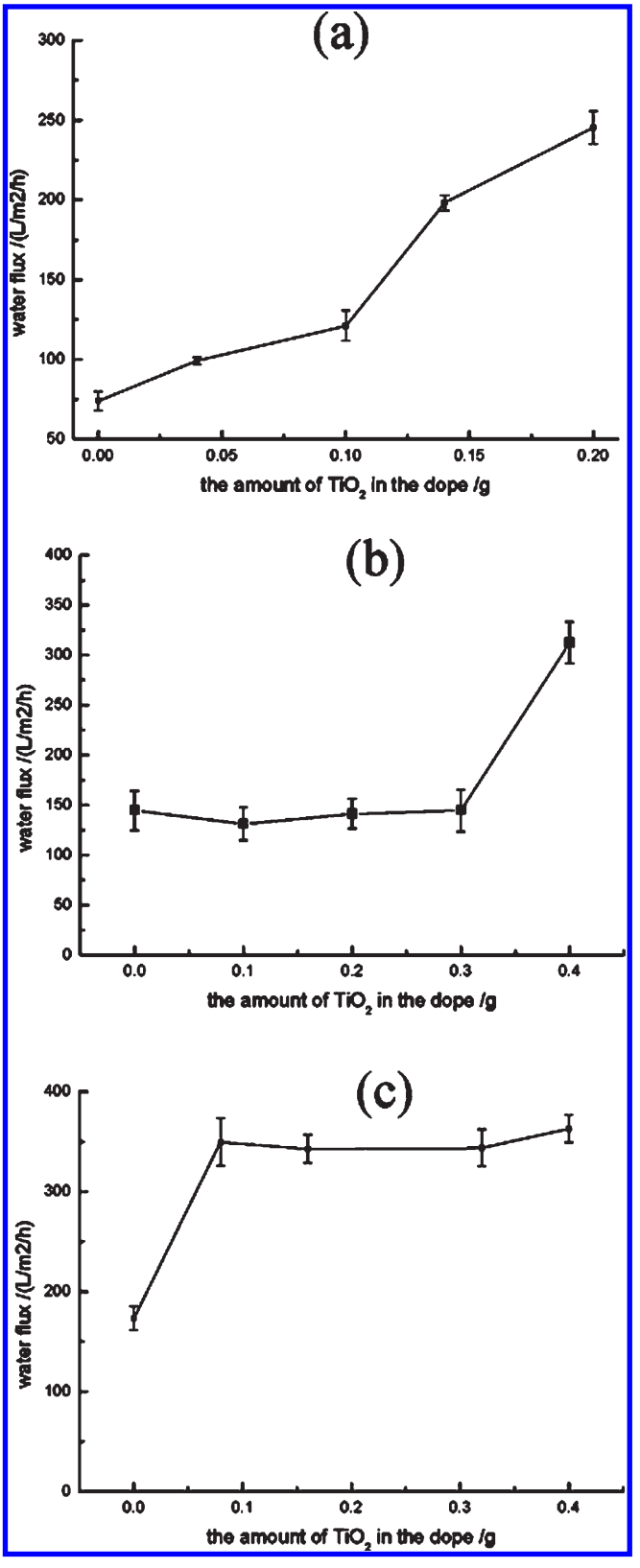

Figure 4. Influence of TiO_2 amount in the casting solution on the performances of membranes made from (a) PVDF, (b) PVDF-*g*-MA, and (c) PVDF-*g*-PAM.

reports the measurements of the mean pore sizes and the mean contact angles of the neat and hybrid membranes.

Table 2. Water Contact Angles and Mean Pore Sizes of Neat and Hybrid Membranes

membrane ID	mean pore size of membrane (μm)	water contact angle* (deg)
PVDF	0.1225	79.4 (1.4)
PVDF/TiO_2-0.04	0.1207	77.2 (1.2)
PVDF/TiO_2-0.1	0.1339	73.5 (2.2)
PVDF/TiO_2-0.14	0.1228	72.1 (1.0)
PVDF/TiO_2-0.2	0.1237	71.6 (0.9)
PVDF-*g*-MA	0.1345	78.9 (1.5)
PVDF-*g*-MA/TiO_2-0.1	0.1441	77.2 (0.8)
PVDF-*g*-MA/TiO_2-0.2	0.1422	71.7 (1.4)
PVDF-*g*-MA/TiO_2-0.3	0.1443	74.2 (0.6)
PVDF-*g*-MA/TiO_2-0.4	0.1359	65.9 (1.6)
PVDF-*g*-PAM	0.1285	73.5 (0.9)
PVDF-*g*-PAM/TiO_2-0.08	0.1192	67.9 (2.1)
PVDF-*g*-PAM/TiO_2-0.16	0.1293	75.3 (1.3)
PVDF-*g*-PAM/TiO_2-0.32	0.1143	73.8 (1.7)
PVDF-*g*-PAM/TiO_2-0.4	0.1142	69.5 (1.5)

* Standard deviation in parentheses.

Figure 4 shows that nano-TiO_2 addition in the casting solutions improved the membranes' water flux. However, the degree of influence of TiO_2 on the membrane performance was different depending on the type of polymer. Table 2 indicates that there was not much difference in pore size between the hybrid membranes and the neat membranes, and the contact angle measurements show that the addition of TiO_2 caused various degrees of decrease of the contact angles. It is generally believed that it is the properties of the membrane skin layer, including the size of its pores and its porosity, that play a key role in determining the membrane performance. As shown in Table 2, the change in pore size was so limited that it was difficult to relate the increase in flux of the hybrid membranes to the change in pore size. However, it was observed that the addition of nano-TiO_2 reduced the thickness of the skin layer, increased the number of pores, and improved the interconnectivity between the pores in the sublayer. Moreover, these changes all contributed to the reduction of the permeating resistance, and this is thought to be the main reason for the larger pure-water flux of the hybrid membranes.[27] It should also be noted that, for the PVDF-*g*-MA/TiO_2 hybrid membranes, the water flux increased obviously only when the amount of nano-TiO_2 addition exceeded 0.3 g, whereas for PVDF-*g*-PAM/TiO_2 hybrid membranes, the water flux stopped increasing with the increase in TiO_2 addition when the amount of TiO_2 added exceeded 0.1 g. The reason behind this phenomenon is still not clear; however, it can be concluded that the nano-TiO_2 addition exerted a significant influence on the structure of the hybrid membranes and, hence, improved their water flux.

At the same time, the change in hydrophilicity also affected the membrane performance. Generally speaking, to a certain degree, the contact angle indicates the surface hydrophilicity of the membranes. Because of the rich hydroxyl groups existing on the nano-TiO_2 surface and the higher affinity of the metal oxide for water, the hydrophilicity of the hybrid membranes' surface layer was improved to different degrees. However, for the hybrid membranes of PVDF-*g*-MA and PVDF-*g*-PAM, the decrease in contact angle (i.e., increase in hydrophilicity) was not correlated

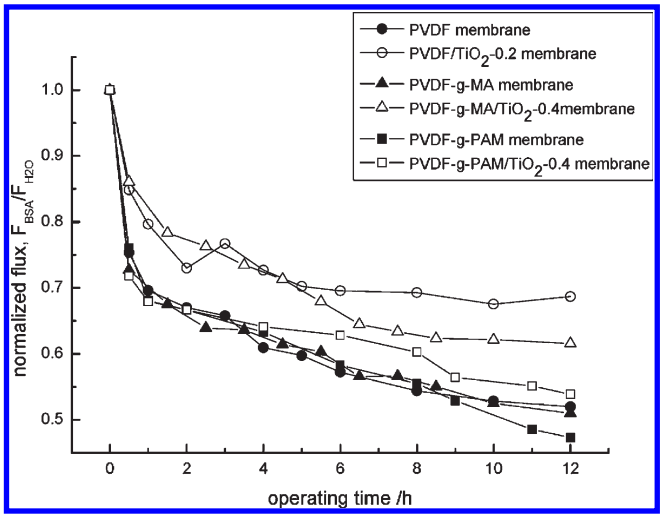

Figure 5. Flux of 0.5 g/L BSA solution (F_{BSA}) divided by the initial pure-water flux (F_{H_2O}) as a function of operating time for neat and hybrid membranes.

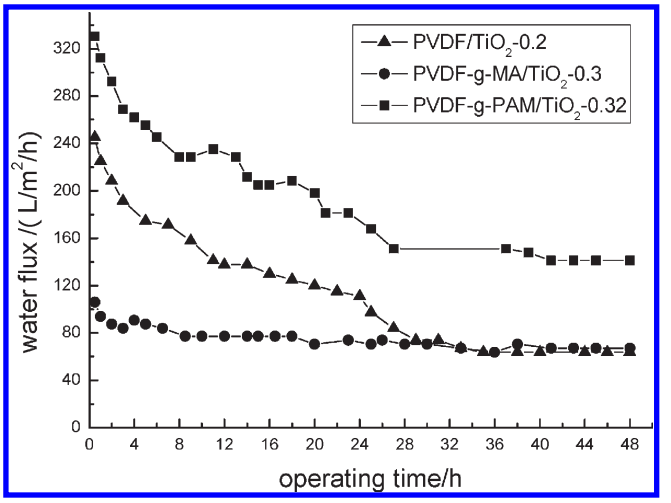

Figure 6. Pure-water flux decline behavior of hybrid membranes during 48-h-long pure-water experiments.

with the increase in TiO_2 amount and the increase in the membrane water flux. Therefore, the improvement in the hydrophilic properties of the membrane surface brought about by nano-TiO_2 addition might have contributed to the increase in water flux of the hybrid membrane; however, its contribution was limited.[28]

Owing to the fact that membrane performance is related not only to the phase inversion process (i.e,. thermodynamic and kinetic factors that play an important role in membrane formation), but also linked to interactions between nano-TiO_2 and polymer, it is quite difficult to make precise predictions about how membranes will perform after the addition of nano-TiO_2 particles.

3.2.2. Antifouling Properties of Neat and Hybrid Membranes. In this study, the following three groups of membranes were selected for comparison: (1) PVDF membranes versus PVDF/TiO_2-0.2 membranes, (2) PVDF-*g*-MA membranes versus PVDF-*g*-MA/TiO_2-0.4 membranes, and (3) PVDF-*g*-PAM membranes versus PVDF-*g*-PAM/TiO_2-0.4 membranes.

Changes in performance for both neat and hybrid membranes in the filtration of BSA protein solution were observed. The results are shown in Figure 5. In this figure, to plot the flux change caused by BSA fouling alone, a normalized BSA flux (i.e, the ratio of the instantaneous BSA flux to the initial pure-water flux measured at the end of the compaction period) was used to analyze the antifouling performance of all of the membranes tested. (Note that, in this article, the initial pure-water flux was measured after 5 h of filtration of deionized water under a pressure of 0.2 MPa.)

Figure 5 reveals that both the neat membranes and the hybrid membranes exhibited a flux decline resulting from fouling. By comparison, the decline in flux demonstrated by the hybrid membranes with TiO_2 addition was rather mild. For example, after 12 h of continuous filtration, the flux of PVDF/TiO_2-0.2 dropped to 68.6% of its initial pure-water flux, indicating that it had better antifouling properties than the neat PVDF membrane, whose flux dropped to 51.9% of the initial pure-water flux. The PVDF-*g*-MA/TiO_2-0.4 membrane, whose flux dropped to 61.6% of the initial pure-water value after 12 h of filtration, had better antifouling properties than the pure PVDF-*g*-MA membrane, whose flux was 51.0% of its initial pure-water flux value. Finally, the flux of the PVDF-*g*-PAM/TiO_2-0.4 hybrid membrane dropped to 53.9% of the initial pure-water flux, which was better than the value of 47.3% for the neat PVDF-*g*-PAM membrane. Moreover, together with the data on membrane contact angles (listed in Table 2), these experimental results indicate that improvement in the membrane surface hydrophilicity contributes to the membrane's antifouling performance.

3.2.3. Stability of Hybrid Membrane Performance in Long-Time Pure-Water Experiments. Because the addition of nano-TiO_2 particles was found to improve the membrane performance, the issue of whether these particles are firmly and stably adhered to the polymer is a factor affecting the stability of membrane performance. To investigate the stability of the adherence of the nano-TiO_2 particles to the polymer and its influence on membrane performance, long-time pure-water permeation experiments and EDS observations of the Ti content on the membrane surface during operation, as well as contact angle measurements of hybrid membranes before and after pure-water permeation, were carried out. The pure-water flux decline behavior of hybrid membranes is plotted in Figure 6.

Figure 6 shows that all three types of hybrid membranes underwent a flux decline. After 48 h of pure-water permeation, the pure-water fluxes of the PVDF/TiO_2-0.2, PVDF-*g*-MA/TiO_2-0.3, and PVDF-*g*-PAM/TiO_2-0.32 membranes dropped from their original values of 245, 106.18, and 330.62 L/(m^2·h) to 63.8, 67.2, and 141.1 L/(m^2·h), respectively. In other words, the water fluxes dropped to only 26.1%, 63.3%, and 42.7% of their initial values.

In these experiments, two main factors might have led to the water flux decline. The first is the compaction of the membrane under pressure of 0.2 MPa, which is a typical phenomenon. The second factor causing hybrid membranes to undergo further decline might be the partial removal of TiO_2 particles off the membrane surface and channel blocking by the TiO_2 particles that came off during the filtration process. Thus, the Ti content was analyzed by EDS during the filtration process. The results are listed in Table 3.

In this study, it was assumed that the nano-TiO_2 particles were evenly distributed in the casting solution. The theoretical Ti content (%) in a hybrid membrane was calculated based on the

Table 3. Ti Contents (wt %) on Polymer/TiO_2 Hybrid Membrane Surface Measured at Different Time Points during the 48-h-Long Pure-Water Permeation Experiments

	run time (h)				
hybrid membrane	0	5	14	25	48
PVDF/TiO_2-0.2	1.05	0.92	–	–	0.93
PVDF-*g*-MA/TiO_2-0.3	2.64	2.45	2.48	–	2.49
PVDF-*g*-PAM/TiO_2-0.32	2.90	2.58	–	2.46	2.46

Table 4. Change in Contact Angle of Hybrid Membranes before and after 48-h-Long Pure-Water Permeation Experiments

	contact angle (deg)	
membrane ID	before permeation test	after permeation test
PVDF/TiO_2-0.2	71.63	81.84
PVDF-*g*-MA/TiO_2-0.3	74.16	81.88
PVDF-*g*-PAM/TiO_2-0.32	73.8	77.24

ratio of the weight of TiO_2 to the total weight of polymer + TiO_2 (as shown in Table 1) and the Ti percentage of the overall mass of a TiO_2 molecule. After the membrane formation process, the theoretical values of the Ti contents in the surface layers of the hybrid membranes PVDF/TiO_2-0.2, PVDF-*g*-MA/TiO_2-0.3, and PVDF-*g*-PAM/TiO_2-0.32 were 1.22%, 1.98%, and 2.31%, respectively. However, as shown in Table 3, the actual values obtained by EDS analysis for PVDF-*g*-MA/TiO_2-0.3 and PVDF-*g*-PAM/TiO_2-0.32 were 2.64% and 2.90%, respectively, which were higher than the theoretical values, whereas the actual value for PVDF/TiO_2 was lower than its theoretical maximum. Studies of the roles of PVDF-*g*-PMAA, PVDF-*g*-AA, and hyperbranched polymers in PVDF membrane modification have revealed the phenomenon of hydrophilic groups migrating toward the membrane surfaces during the membrane formation process.[29−31] In this study, it was believed that the hydrophilic groups (i.e., MA and PAM groups) showed a similar tendency to migrate toward the membrane surface after being grafted onto PVDF, and at the same time, the nano-TiO_2 particles also moved under a certain force toward the membrane surface together with the hydrophilic groups, leading to the enrichment of nano-TiO_2 particles near the membrane surface. For PVDF/TiO_2-0.2, the fact that its actual Ti content value was lower than the theoretical value can be attributed to the partial loss of TiO_2 particles.

The results of the EDS analysis of Ti content shown in Table 3 indicate that some of the TiO_2 particles were removed from the membrane during the 48-h-long operating process, whereas the remaining TiO_2 particles were immobilized in the membrane. Certain interactions between TiO_2 and polymer might have caused the immobilization of TiO_2 particles.

In the meantime, changes in contact angle before and after the 48-h continuous operation were compared among these hybrid membranes. The results are presented in Table 4.

Table 4 shows that the contact angle for all three types of hybrid membranes increased after the 48-h continuous operation. It is believed that the main reason for this phenomenon is the removal of some TiO_2 particles embedded in the membrane surface. At the same time, it was also noticed that, after the 48-h operation, the hybrid membranes had a higher contact angle than the neat membranes, as shown in Table 2. This phenomenon might be caused by the removal of TiO_2 during the experiments, resulting in changes in the hydrophilicity and morphology.

The above experimental results suggest that the loss of TiO_2 nanoparticles affected the stability of the hybrid membrane performance.

3.3. XPS Analysis. As discussed in section 3.2.3, the loss of TiO_2 particles would lower the hybrid membrane performance. In a search for ways to prepare high-performance TiO_2 hybrid membranes, researchers have revealed that nano-TiO_2 particles can be bonded with carboxylate or sulfonic acid groups through self-assembly or through the formation of H bonds between carbonyl groups and the surface hydroxyl groups of TiO_2.[32] In this study, to explore potential or possible interactions between the nano-TiO_2 particles and the polymer, XPS was employed for the analytical characterization of neat and hybrid membranes. To avoid interference, PEG400 was not used in preparing the membrane samples for XPS analysis.

Survey XPS spectra for each of the three hybrid membranes were measured, and parts a−c of Figure 7 present survey XPS spectra of PVDF/TiO_2-0.2, PVDF-*g*-MA/TiO_2-0.3, and PVDF-*g*-PAM/TiO_2-0.32 membranes, respectively, showing the positions of all of the photoelectron peaks, which are in agreement with the values reported by other researchers. The presence of Ti peaks provides evidence that TiO_2 were immobilized on the hybrid membrane surface through certain interactions.

In addition to the survey spectra, high-resolution XPS studies were also carried out to better understand the possible interactions between polymer and TiO_2. Figure 8 presents high-resolution XPS spectra of neat and hybrid membranes.

Parts a and b of Figure 8 are the C 1s and F 1s XPS spectra, respectively, of PVDF and PVDF/TiO_2 membranes. They show that the hybrid membrane had almost the same C 1s and F 1s binding energy values as the neat membrane. This indicates that there was no chemical reaction between TiO_2 and polymer, suggesting that the nano-TiO_2 particles embedded in the membrane surface layer were merely intertwined with the polymer chains.

Figure 8c is the O 1s XPS spectra of the surfaces of the PVDF-*g*-MA and PVDF-*g*-MA/TiO_2 membranes. The O 1s core-level spectrum for the PVDF-*g*-MA membrane includes two components, both of which are assigned to the grafted maleic anhydride unit: the component with a binding energy of 532.4 eV is for C═O, and the other one with a binding energy of 533.8 eV is for C−O−C. Both binding energy values are in agreement with reported values.[33] Moreover, the relative area ratio of the peak of C═O to that of C−O−C is about 2:1, which is in agreement with the structure of MA. However, compared with that of the neat membrane, the O 1s XPS spectrum of the PVDF-*g*-MA/TiO_2 hybrid membrane indicates that the addition of TiO_2 made a difference. The XPS spectrum contains not only three O 1s peaks, for the C═O and C−O−C groups in anhydride and Ti−O in TiO_2 at 530.3 eV, but also a new unknown O 1s peak at 531.5 eV.[34] The new peak is supposed to arise from a C═O···Ti complex, and its formation might be attributable to the coordinate reaction between partial C═O and nano-TiO_2 particles.

Parts d and e of Figure 8 are the N 1s and O 1s XPS spectra, respectively, of the surfaces of PVDF-*g*-PAM and PVDF-*g*-PAM/TiO_2 membranes. Upon comparison of the N 1s binding energy of the PVDF-*g*-PAM membrane with that of the PVDF-*g*-PAM/TiO_2

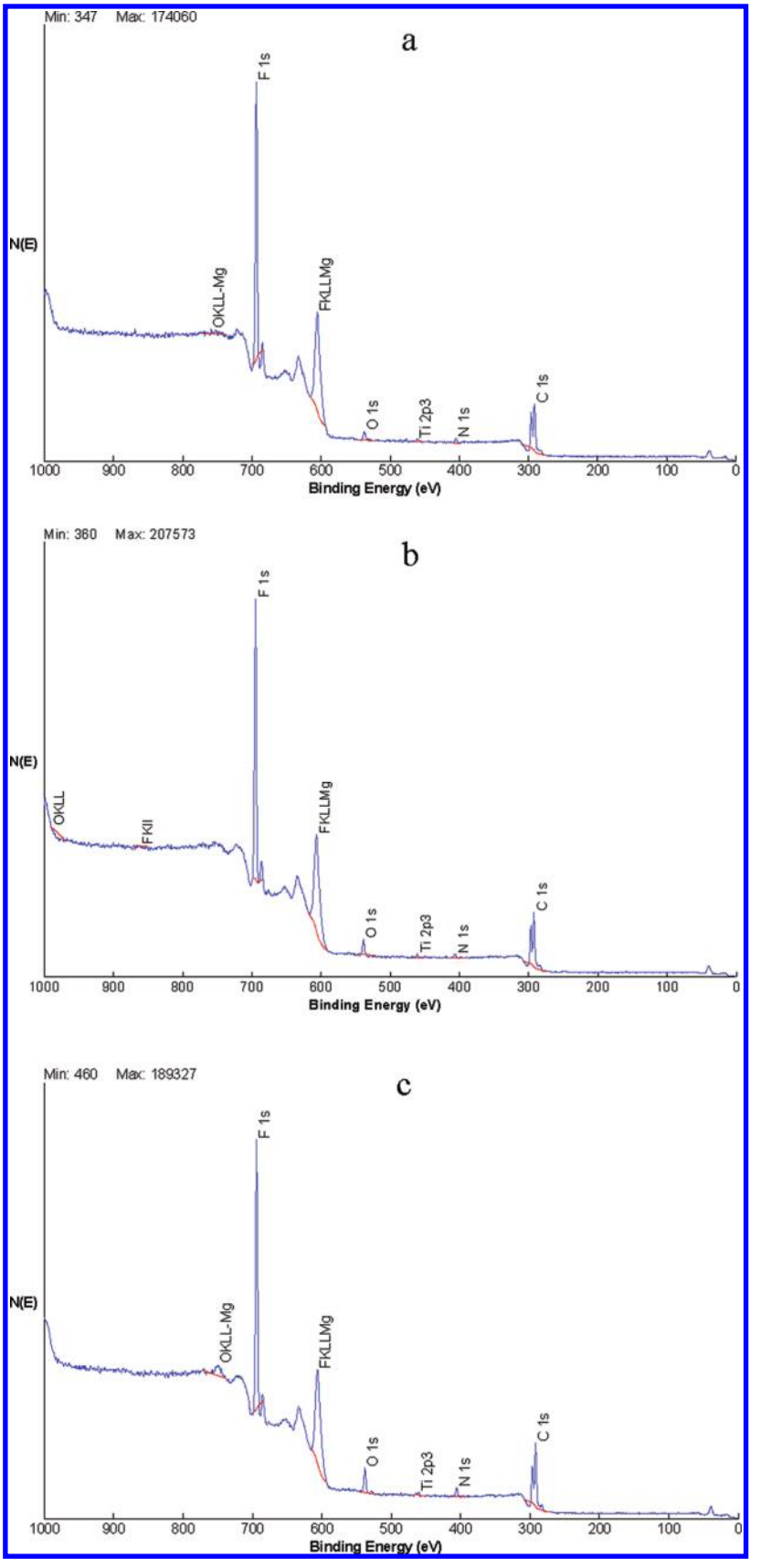

Figure 7. Survey XPS spectra of (a) PVDF/TiO_2-0.2, (b) PVDF-*g*-MA/TiO_2-0.3, and (c) PVDF-*g*-PAM/TiO_2-0.32 membranes.

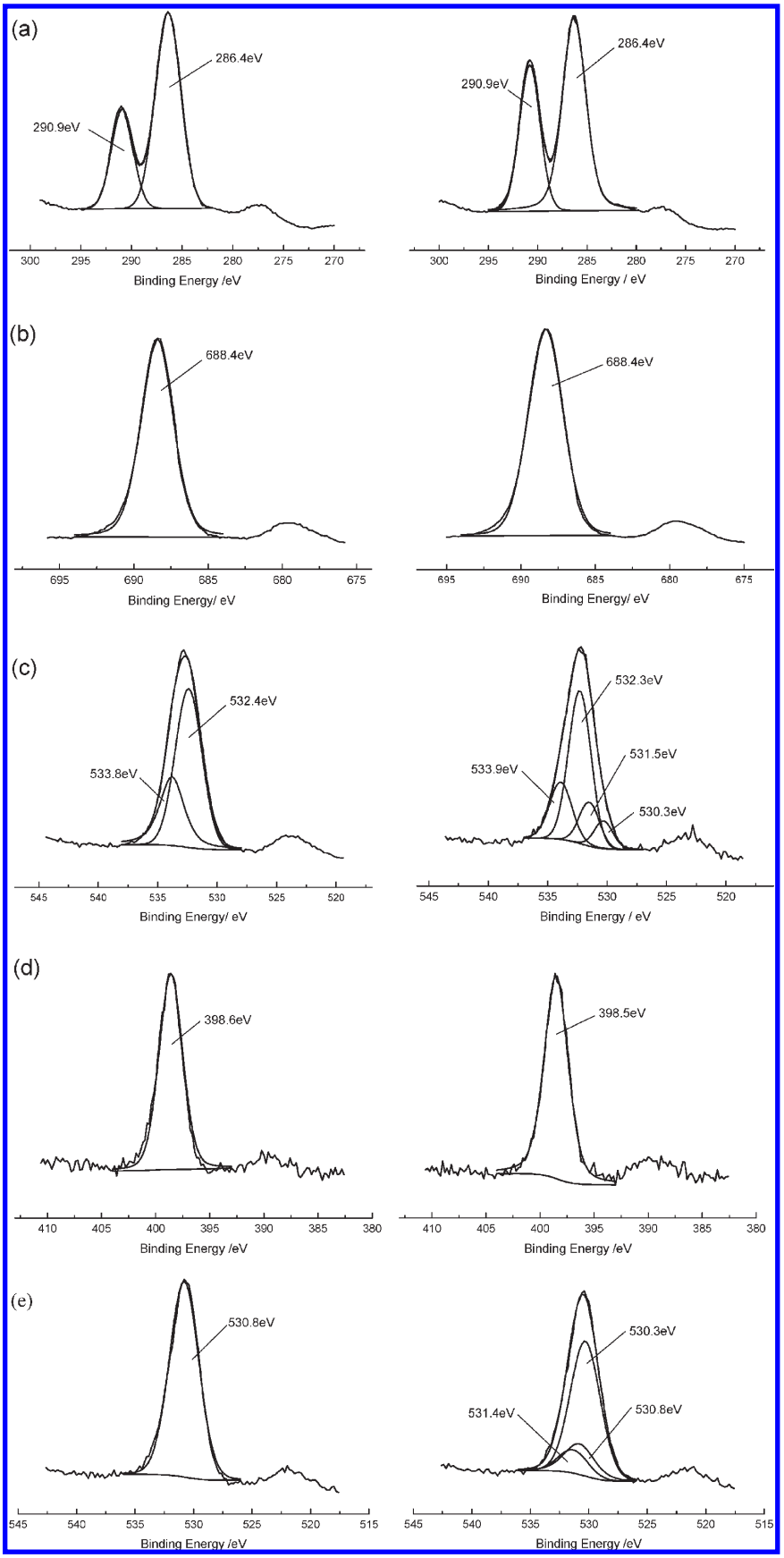

Figure 8. XPS spectra of (left) neat and (right) polymer/TiO_2 hybrid membrane surfaces. (a) C 1s and (b) F 1s XPS spectra of PVDF and PVDF/TiO_2-0.2 membrane surfaces. (c) O 1s XPS spectra of PVDF-*g*-MA and PVDF-*g*-MA/TiO_2-0.3 membrane surfaces. (d) N 1s and (e) O 1s XPS spectra of PVDF-*g*-PAM and PVDF-*g*-PAM/TiO_2-0.32 membrane surfaces.

membrane, no obvious binding energy (BE) shift can be observed. This indicates that amide groups did not take part in the reaction with nano-TiO_2 particles.

As seen in Figure 8e, the peak at 530.8 eV is assigned to C═O in PAM for the neat membrane. In the case of the hybrid membrane, the O 1s peak can be fitted with three peaks: a peak at 530.3 eV assigned to O 1s in TiO_2, a peak at 530.8 eV assigned to O atom in C═O in PAM, and a peak at 531.4 eV that can be assumed to be the new complex of C═O···Ti.[35]

Based on the discussions above, one can reach the conclusion that nanoparticles can be immobilized on the surface of membranes in two ways: one involves the formation of a relatively stable chemical structure resulting from the reaction between nano-TiO_2 particles and functional groups in the polymer, such as C═O in maleic anhydride or acryl amide; the other involves embedding of nano-TiO_2 particles in the membrane as a result of their intertwining with polymer chains during the hybrid membrane preparation process.

4. CONCLUSIONS

In this article, nano-TiO_2 particles were blended with PVDF, PVDF-*g*-MA, and PVDF-*g*-PAM to prepare embedded polymer/TiO_2 hybrid membranes using the phase inversion method.

SEM images showed that the formation of large macrovoids in the hybrid membrane was suppressed. Magnified images of the upper part of the hybrid membrane structure show that, with an increase in the TiO_2 content, the thickness of the skin layer decreased, the number of pores increased, and the connectivity between the pores improved. Although the membrane pore size did not change much after the addition of nano-TiO_2, the water flux of hybrid membranes increased because of the change in the skin layer and the sublayer structure of the hybrid membranes. The EDX mapping indicated the TiO_2 were distributed evenly in the membrane surface.

The membrane fouling experiments indicated that the antifouling performance of hybrid membranes was improved by the introduction of TiO_2 into the membranes.

Over the 48 h-long pure-water experiments, hybrid membranes underwent a decrease in the water flux and increase in the contact angle. EDS analysis confirmed the loss of TiO_2 nanoparticles during continuous filtration. The loss of TiO_2 nanoparticles would influence the stability of hybrid membrane performance.

The XPS analysis indicated that nano-TiO_2 particles were immobilized on the membrane surface through the formation of a C═O···Ti complex resulting from the reaction of C═O in MA or PAM groups in the polymer with nano-TiO_2 particles and/or through the intertwining of nano-TiO_2 particles with polymer chains.

AUTHOR INFORMATION

Corresponding Author

*E-mail: luxiaofeng@sinap.ac.cn.

ACKNOWLEDGMENT

Financial support for this work was provided by the Shanghai Municipal Science and Technology Committee (Contract 08231200300) and the Knowledge Innovation Program of Chinese Academy of Sciences. Special thanks go to Ms. Lu Ying, professor at Ningbo University, who generously helped us with the pore size measurements.

REFERENCES

(1) Doyen, W.; Leysen, R.; Mottar, J.; Waes, G. New composite tubular membranes for ultrafiltration. *Desalination* **1990**, *79*, 163.

(2) Kwak, S. Y.; Kim, S. H.; Kim, S. S. Hybrid organic/inorganic reverse osmosis (RO) membrane for bactericidal anti-fouling. 1. Preparation and characterization of TiO_2 nanopartical self assembled aromatic polyamide thin-film-composite (TFC) membrane. *Environ. Sci. Technol.* **2001**, *35*, 2388.

(3) Kim, S. H.; Kwak, S.-Y.; Sohn, B.-H.; Park, T. H. Design of TiO_2 nanoparticle self-assembled aromatic polyamide thin-film-composite (TFC) membrane as an approach to solve biofouling problem. *J . Membr. Sci.* **2003**, *211*, 157.

(4) Moaddeb, M.; Koros, W. J. Gas transport properties of thin polymeric membranes in the presence of silicon dioxide particles. *J . Membr. Sci.* **1997**, *125*, 143.

(5) Zimmerman, C. M.; Singh, A.; Koros, W. J. Tailoring mixed matrix composite membrane for gas separations. *J . Membr. Sci.* **1997**, *137*, 145.

(6) Kong, Y.; Du, H.; Yang, J.; Shi, D.; Wang, Y.; Zhang, Y.; Xin, W. Study on polyimide/TiO_2 nanocomposite membranes for gas separation. *Desalination* **2002**, *146*, 49.

(7) Vankelecom, I. F. J.; Debeukelaer, S.; Uytterhoeven, J. B. Sorption and pervaporation of aroma compounds using zeolite-filled PDMS membranes. *J. Phys. Chem. B* **1997**, *101*, 5186.

(8) Boom, J. P.; Punt, I. J. M.; Zwijnenberg, H.; de Boer, R.; Bargeman, D.; Smolders, C. A.; Strathmann, H. Transport through zeolite filled polymeric membranes. *J . Membr. Sci.* **1998**, *138*, 237.

(9) Chen, X.; Ping, Z. H.; Long, Y. C. Separation properties of alcohol−water mixture through silicalite-I-filled silicone rubber membranes by pervaporation. *J. Appl. Polym. Sci.* **1998**, *67*, 629.

(10) Genne, I.; Kuypers, S.; Leysen, R. Effect of the addition of ZrO_2 to polysulfone based UF membranes. *J . Membr. Sci.* **1996**, *113*, 343.

(11) Schaep, J.; Vandecasteele, C.; Leysen, R.; Doyen, W. Salt retention of Zirfon membranes. *Sep. Purif. Technol.* **1998**, *14*, 127.

(12) Aerts, P.; Genne, I.; Kuypers, S.; Leysen, R.; Vankelecom, I. F. J.; Jacobs, P. A. Polysulfone−aerosil composite membranes: Part 2. The influence of the addition of aerosil on the skin characteristics and membrane properties. *J . Membr. Sci.* **2001**, *178*, 1.

(13) Bottino, A.; Capannelli, G.; D'Asti, V.; Piaggio, P. Preparation and properties of novel organic−inorganic porous membranes. *Sep. Purif. Technol.* **2001**, *22*−*23*, 269.

(14) Aerts, P.; Greenberg, A. R.; Leysen, R.; Krantz, W. B.; Reinsch, V. E.; Jacobs, P. A. The influence of filler concentration on the compaction and filtration properties of Zirfon-composite ultrafiltration membranes. *Sep. Purif. Technol.* **2001**, *22*−*23*, 663.

(15) Bottino, A.; Caparmelli, G.; Comite, A. Preparation of novel porous PVDF−ZrO_2 composite membranes. *Desalination* **2002**, *146*, 35.

(16) Molinari, R.; Mungari, M.; Drioli, E.; Di Paola, A.; Loddo, V.; Palmisano, L.; Schiavello, M. Study on a photocatalytic membrane reactor for waste purification. *Catal. Today* **2000**, *55*, 71.

(17) Molinari, R.; Grande, C.; Drioli, E.; Palmisano, L.; Schiavello, M. Photocatalytic membrane reactors for degradation of organic pollutants in water. *Catal. Today* **2001**, *67*, 273.

(18) Molinari, R.; Palmisano, L.; Drioli, E.; Schiavello, M. Studies on various reactor configurations for coupling photocatalysis and membrane process in water purification. *J . Membr. Sci.* **2002**, *206*, 399.

(19) Bae, T. H.; Tak, T. M. Effect of TiO_2 nanoparticles on fouling mitigation of ultrafiltration membranes for activated sludge filtration. *J . Membr. Sci.* **2005**, *249*, 1.

(20) Shin, H.; Collins, R. J.; De Guire, M. R.; Heuer, A. H.; Sukenik, C.N. *J. Mater. Res.* **1995**, *10*, 692.

(21) Shin, H.; Collins, R. J.; De Guire, M. R.; Heuer, A. H.; Sukenik, C.N. *J. Mater. Res.* **1995**, *10*, 699.

(22) Liu, Y.; Wang, A.; Claus, R. Molecular self-assembly of TiO_2/polymer nanocomposite films. *J. Phys. Chem. B* **1997**, *101*, 1385.

(23) Bae, T. H.; Tak, T. M. Preparation of TiO_2 self-assembled polymeric nanocomposite membrane and examination of their fouling mitigation effects in a membrane bioreactor system. *J. Membr. Sci.* **2005**, *266*, 1.

(24) Deng, B.; Li, J.; Hou, Z.; Yao, S.; Shi, L.; Liang, G.; Sheng, K. Microfiltration membranes prepared from polyethersulfone powder grafted with acrylic acid by simultaneous irradiation and their pH dependence. *Radiat. Phys. Chem.* **2008**, *77*, 898.

(25) Deng, B.; Yang, X.; Xie, L.; Li, J.; Hou, Z.; Yao, S.; Liang, G.; Sheng, K.; Huang, Q. Microfiltration membranes with pH dependent property prepared from poly(methacrylic acid) grafted polyethersulfone powder. *J. Membr. Sci.* **2009**, *330*, 363.

(26) McKelvey, S. A.; Koros, W. J. Phase separation, vitrification, and the manifestation of macrovoids in polymeric asymmetric membranes. *J. Membr. Sci.* **1996**, *112*, 29.

(27) Cao, X.; Ma, J.; Shi, X.; Ren, Z. Effect of TiO_2 nanoparticle size on the performance of PVDF membrane. *Appl. Sur. Sci.* **2006**, *253*, 2003.

(28) Yu, L. Y.; Shen, H. M.; Xu, Z. L. PVDF−TiO_2 composite hollow fiber ultrafiltration membrane prepared bu TiO_2 sol−gel method and blending method. *J. Appl. Polym. Sci.* **2009**, *113*, 1763.

(29) Hester, J. F.; Olugebefola, S. C.; Mayes, A. M. Preparation of pH-responsive polymer membranes by self-organization. *J. Membr. Sci.* **2002**, *208*, 375.

(30) Ying, Lei; Kang, E. T.; Neoh, K. G. Synthesis and Characterization of Poly(*N*-isopropylacrylamide)-*graft*-Poly(vinylidene fluoride) Copolymers and Temperature-Sensitive Membranes. *Macromolecules* **2002**, *35*, 673.

(31) Zhao, Y. H. Modification of porous PVDF membrane by hyperbranched polymer. Ph.D. Thesis, Zhejiang University, Hangzhou, China, 2008.

(32) Lee, S. J.; Han, S. W.; Yoon, M.; Kim, K. Adsorption characteristics of 4-dimethylaminobenzoic acid on silver and titania: Diffuse reflectance infrared Fourier transform spectroscopy study. *Vib. Spectrosc.* **2000**, *24*, 265.

(33) Beamson, G.; Briggs, D. *High Resolution XPS of Organic Polymers: The Scienta ESCA300 Database*; John Wiley & Sons: New York, 1992.

(34) Moulder, J. F.; Stickle, W. F.; Sobol, P. E.; Bomben, K. D. In *Handbook of X-ray Photoelectron Spectroscopy*; Chastain, J., Ed.; Perkin-Elmer Corporation: Wellesley, MA, 1992.

(35) Yu, G.; Chen, H.; Zhang, X.; Jiang, Z.; Huang, B. Polymer-supported titanium catalysts for syndiotactic polymerization of styrene. *J. Polym. Sci. A: Polym. Chem.* **1996**, *34*, 2237.